HHS Public Access

Author manuscript

Mol Cell. Author manuscript; available in PMC 2021 June 18.

Published in final edited form as:

Mol Cell. 2020 June 18; 78(6): 1252–1263.e3. doi:10.1016/j.molcel.2020.04.009.

Mechanistic insight into crossing over during mouse meiosis

Shaun E. Peterson[a], **Scott Keeney**[b,c], **Maria Jasin**[a,†]

[a]Developmental Biology Program, Memorial Sloan Kettering Cancer Center, New York, NY, USA

[b]Molecular Biology Program, Memorial Sloan Kettering Cancer Center, New York, NY, USA

[c]Howard Hughes Medical Institute, Memorial Sloan Kettering Cancer Center, New York, NY, USA

SUMMARY

Crossover recombination is critical for meiotic chromosome segregation, but how mammalian crossing over is accomplished is poorly understood. Here we illuminate how strands exchange during meiotic recombination in male mice, by analyzing patterns of heteroduplex DNA in recombinant molecules preserved by the mismatch correction deficiency of *Msh2*$^{-/-}$ mutants. Surprisingly, MSH2-dependent recombination suppression was not evident. However, a substantial fraction of crossover products retained heteroduplex DNA and some provided evidence of MSH2-independent correction. Biased crossover resolution was observed, consistent with asymmetry between DNA ends in earlier intermediates. Many crossover products yielded no heteroduplex DNA, suggesting dismantling by D-loop migration. Unlike the complexity of crossovers in yeast, these simple modifications of the original double-strand break repair model—asymmetry in recombination intermediates and D-loop migration—may be sufficient to explain most meiotic crossing over in mice while also addressing long-standing questions related to Holliday junction resolution.

Graphical Abstract

To whom correspondence should be addressed: Scott Keeney: s-keeney@ski.mskcc.org. †Lead Contact: Maria Jasin: m-jasin@ski.mskcc.org.

AUTHOR CONTRIBUTIONS

SEP performed all of the experiments. SEP, SK, and MJ conceived of the research and designed the experiments. SEP and MJ wrote the manuscript with input from SK.

DECLARATION OF INTERESTS

The authors declare no competing interests.

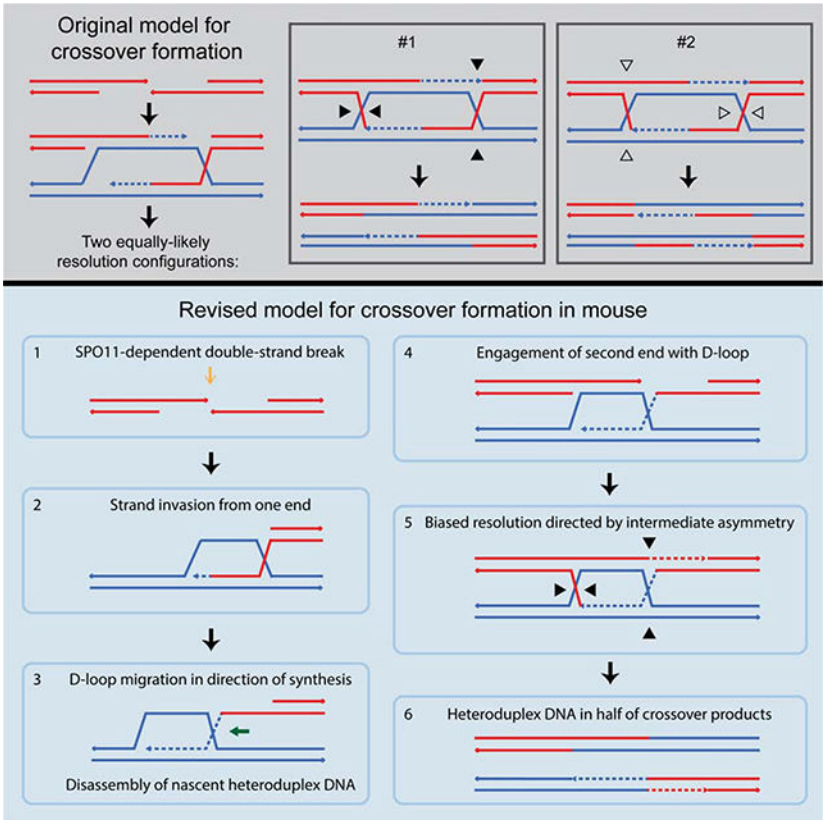

eTOC blurb

An eTOC blurb should also be included that is no longer than 50 words describing the context and significance of the findings for the broader journal readership. When writing this paragraph, please target it to non-specialists by highlighting the major conceptual point of the paper in plain language, without extensive experimental detail. The blurb must be written in the third person and refer to “First Author et al.”

Crossover formation is essential for gamete viability, yet our understanding of mammalian mechanisms largely relies on inference from yeast. Peterson et al. illuminate mechanisms of crossover formation, including commonalities with yeast while distinguishing mammalian-specific differences. This fine-scale study of recombination intermediates allowed revision of the canonical model of crossover formation in mice.

INTRODUCTION

Crossing over has an essential mechanical role at the first meiotic division by ensuring the segregation of homologous chromosomes (Hunter, 2015). Meiotic recombination is also a critical driver of genetic diversity and genome evolution (Spencer et al., 2006; Pratto et al., 2014; Dapper and Payseur, 2017; Veller et al., 2019). Despite decades of study, however, key questions remain about the mechanism of crossing over, particularly in mammalian meiosis. In fungi, insights have come from analysis of heteroduplex DNA—consisting of a strand from each homolog—that arises during crossover formation, correction of which leads to

gene conversion. The position and length of heteroduplex DNA can reveal how DNA strand information is exchanged during the recombination process, but the analytical power of heteroduplex DNA structures of recombination intermediates remains largely untapped in mammals.

Meiotic recombination is initiated by the formation of programmed double-strand breaks (DSBs) (Lam and Keeney, 2015). After resection, one DNA end invades the homolog to form a displacement (D) loop, which then captures the second DNA end to form a double Holliday junction (Gray and Cohen, 2016). Although they involve distinct biochemical activities, both steps—strand invasion and second end capture—result in the formation of heteroduplex DNA. Szostak and colleagues proposed that double Holliday junction resolution gives rise to two crossover and two noncrossover configurations, depending on the placement of paired nicks at each junction (Szostak et al., 1983). Subsequent studies in yeast and mice demonstrated, rather, that most noncrossovers arise by mechanisms distinct from double Holliday resolution (Gilbertson and Stahl, 1996; Allers and Lichten, 2001a; Wu and Hickson, 2003; McMahill et al., 2007; Cole et al., 2014). However, double Holliday junction resolution is still considered to be critical to crossover formation (Collins and Newlon, 1994; Schwacha and Kleckner, 1995; Allers and Lichten, 2001b).

In mitotic and meiotic yeast cells, mismatches in heteroduplex DNA are corrected by Msh2-dependent mismatch repair pathways. The mismatch repair machinery also suppresses recombination between non-identical sequences through heteroduplex rejection (Borts et al., 2000; Spies and Fishel, 2015; Chakraborty and Alani, 2016; Tham et al., 2016). Thus, in the absence of mismatch repair factors like Msh2, recombination between non-identical sequences is elevated and recombination products often show evidence of unrepaired heteroduplex DNA (Datta et al., 1996; Chen and Jinks-Robertson, 1999). In mammals, MSH2 plays similar roles in heteroduplex rejection and correction of mismatches in heteroduplex DNA in mitotic cells (de Wind et al., 1995; Elliott and Jasin, 2001), although these roles have yet to be explored in meiosis.

Genome-wide studies in budding yeast have cataloged thousands of crossover and noncrossover products (Chen et al., 2008; Mancera et al., 2008; Mancera et al., 2011; Anderson et al., 2015), including more recently in *msh2Δ* mutants displaying heteroduplex DNA retention (Martini et al., 2011; Marsolier-Kergoat et al., 2018). These latter studies observed complex heteroduplex DNA patterns in crossovers, leading to further modifications to the original DSB repair model including D-loop migration, double-Holliday junction migration, nick translation, template switching, and biased Holliday junction resolution.

Here, we probed mechanisms of meiotic recombination in mouse spermatocytes by defining spatial patterns of heteroduplex DNA through a comprehensive analysis of meiotic recombination products in *Msh2*$^{-/-}$ F1 hybrid mice. We recovered hundreds of meiotic crossover and noncrossover products at two DSB hotspots with different levels of sequence divergence. Surprisingly, loss of MSH2 did not substantially change the recombination frequency. However, MSH2 plays an important role in mismatch correction during meiosis, allowing us to infer the presence of heteroduplex DNA. For an asymmetric hotspot in which DSB formation occurs mostly on one homolog, heteroduplex DNA was primarily observed

on one side of recombinant molecules, suggesting that double Holliday junction resolution is surprisingly biased toward one of the possible configurations. Heteroduplex DNA presence was inferred in only a subset of crossover products and, moreover, these products had exchange points closer to the hotspot center than those without heteroduplex DNA. These features suggest an underlying asymmetry in the way the two DNA ends engage with the homolog and point to mechanisms to disassemble heteroduplex DNA at one of the DNA ends. We incorporate these features into a simple model of meiotic crossover formation which shares aspects with models proposed in other organisms, providing a framework for understanding fundamental meiotic recombination mechanisms from yeast to mammals.

RESULTS

Recombination frequencies at a symmetric hotspot are similar in wild-type and *Msh2*$^{-/-}$ mice

Msh2$^{-/-}$ and wild-type mice have equivalent numbers of MLH1 foci during meiosis (Figure S1), suggesting that crossover numbers are not globally affected. However, it is not clear if loss of MSH2 affects crossover placement to favor less polymorphic hotspots. To address this, we performed recombination assays at two hotspots using sperm from wild-type and *Msh2*$^{-/-}$ F1 hybrid mice which contain homologous chromosomes originating from two inbred strains, A/J (A) and DBA/2J (D).The *C1* hotspot on chromosome 1 has a DSB hotspot spanning ~200 bp, with a center of DSB activity at bp 78,590,954 in C57BL/6J (B6) mice (GRCm38; relative position = 0 bp; formerly termed the “central” hotspot (de Boer et al., 2015; Lange et al., 2016)) (Figure 1A). The A and D mouse strains have identical sequences at the PRDM9 consensus motif to each other (and to B6) at this hotspot (Figure S2A), such that the *C1* hotspot is symmetric, with DSB formation expected to occur at equal frequency on both homologs. Within the 2.0 kb assayed, A and D have 0.6% polymorphism density, mostly from single nucleotide polymorphisms (SNPs), although a 16-bp indel is present ~20 bp upstream of the hotspot center (Figure 1A, Figure S2A). The next closest polymorphism to the hotspot center is a SNP located 74 bp downstream.

To specifically amplify crossover products at *C1*, nested PCR was performed on small pools of sperm DNA (~230 sperm per pool on average) using allele-specific forward and reverse primers of opposite haplotypes (i.e., A to D or D to A; Figure 1B–D, Figure S3A). To map exchange points, crossover products were probed with allele-specific oligonucleotides to identify the parent-of-origin of the polymorphisms. The 16-bp indel adjacent to the hotspot center was genotyped by PCR (Figure S2A).

We analyzed ~9×10^5 sperm per genotype from two sets of littermates and recovered 308 positive wells with crossover products from wild type and 326 from *Msh2*$^{-/-}$ for Poisson-adjusted frequencies of 0.071% and 0.077%, respectively (p=0.31, Fisher’s exact test; Figure 1B; Table S1). Although some variation was noted between the pairs of mice, this was unrelated to MSH2 status (Table S1). The similar frequencies suggested that neither density nor positions of polymorphisms trigger a significant MSH2-dependent suppression of recombination.

As expected for reciprocal exchanges, the frequencies were similar for both the A-to-D and D-to-A orientations for wild-type and *Msh2*$^{-/-}$ mice (Figure 1C,D). Crossover activity was determined by mapping the exchange interval for each crossover product (Figure 1B–D; Figure S3C). Broadly similar maps were observed for each orientation and for both orientations combined for wild-type and *Msh2*$^{-/-}$ mice, as expected for a symmetric hotspot with similar DSB activity on both chromosomes.

To determine whether MSH2 affects noncrossover products at *C1*, nested PCR was performed on small pools of sperm DNA (~ 30 or 60 sperm genomes per pool on average) using allele-specific forward and universal reverse primers (Figure S3B). From ~3×10^4 sperm per genotype, we recovered 50 wells with a noncrossover product from wild type and 60 from *Msh2*$^{-/-}$ for Poisson-adjusted frequencies of 0.338% and 0.387%, respectively (p=0.51, Fisher's exact test; Figure 1E,F, Table S2).

More noncrossover products were identified on the D chromosome than the A chromosome, but note that the 16-bp indel was genotyped only on the D chromosome. Each conversion tract from wild-type mice contained a single polymorphism, while five tracts in *Msh2*$^{-/-}$ contained contiguous conversions, which are potential co-conversions (p=0.06, Fisher's exact test). However, two wells from wild-type mice contained two non-contiguous conversions (asterisks, Figure 1E), suggesting distinct noncrossovers, which is within the range for more than one event in the same well, as predicted assuming a Poisson distribution (Table S2).

A highly polymorphic, asymmetric hotspot also shows similar recombination frequencies in wild-type and *Msh2*$^{-/-}$ mice

Results at *C1* suggest that MSH2-dependent heteroduplex rejection either does not occur during meiosis or that the density of mismatches at *C1* is not high enough to trigger a MSH2-dependent response. To investigate the latter possibility, we examined another well-characterized hotspot, *A3* (Cole et al., 2010; Cole et al., 2014). *A3* is on the distal end of chromosome 1, with the DSB hotspot spanning ~250 bp with the center of DSB activity at bp 160,025,733 in B6 (relative position = 0 bp; Figure 2A). Due to polymorphisms within the consensus binding site (Figure S2B), PRDM9 binds with the hierarchy D > B6 > A at *A3* (Cole et al., 2014), such that in F1 hybrids this hotspot is asymmetric, with the majority of DSBs occurring on the D chromosome. Within the 2.4 kb assayed, A and D have 1.8% polymorphism density—about 3-fold higher than the *C1* hotspot—with 41 typed polymorphisms. Other than SNPs, polymorphisms include 2-bp and 3-bp polymorphisms, and three small indels (Figure 2A, Figure S2B).

We recovered 483 positive wells with crossover products from 1.7×10^6 wild-type sperm and 474 positive wells from 1.6×10^6 *Msh2*$^{-/-}$ sperm, among three littermate pairs, for combined Poisson-adjusted frequencies of 0.061% and 0.062%, respectively (p=0.73, Fisher's exact test; Figure 2B, Table S1). Therefore, MSH2 also does not significantly affect crossover frequency at this highly polymorphic hotspot. A-to-D exchanges occurred with greater frequency to one side of the hotspot center (Figure 2C) and D-to-A exchanges to the other side (Figure 2D), as expected for an asymmetric hotspot with DSB formation primarily on one chromosome. Crossover maps were also generally similar between wild type and

mutant, although we note more exchanges in *Msh2*$^{-/-}$ in the intervals flanking the 12-bp indel at the hotspot center, possibly indicating that this indel is affecting the exchange position more strongly in the mutant.

As with crossovers, the noncrossover frequency at *A3* is not clearly affected by MSH2. We identified 136 wells with a noncrossover product from 6×10^4 wild-type sperm and 173 wells from 7×10^4 *Msh2*$^{-/-}$ sperm, among three littermate pairs, for combined Poisson-adjusted frequencies of 0.48% and 0.51%, respectively (p=0.42, Fisher's exact test; Figure 2E,F, Table S2). Some variability was noted in the frequencies of noncrossovers on the two chromosomes. In particular, *Msh2*$^{-/-}$ mice had a third fewer noncrossovers on the A chromosome and fifty percent more noncrossovers on the D chromosome, although the variability was largely due to one mouse in the three littermate pairs (Table S2), and may be attributable to the lower sensitivity of the noncrossover assay due to the excess of amplified parental DNA. For both genotypes, the noncrossover frequency was higher on the D chromosome than the A chromosome, as expected from better PRDM9 binding to the *A3* hotspot on the D chromosome.

In both genotypes, the A chromosome showed a dispersed noncrossover pattern across the interval (Figure 2E), while the D chromosome had a more clustered pattern near the hotspot center (Figure 2F), as previously observed (Cole et al., 2010). A fraction of wells contained non-contiguous conversions, suggesting two (or more) independent noncrossovers in both wild type and mutant (asterisks, Figure 2E,F), as predicted by the Poisson distribution (Table S2). Conversion of contiguous polymorphisms was also seen in noncrossovers from both wild type and *Msh2*$^{-/-}$ (29% and 21%, respectively), especially on the D chromosome at the four most central polymorphisms.

MSH2-dependent correction of heteroduplex DNA within crossover products

We identified three types of crossover products (Figure 3A; Figure S3C): simple, with one switch between parental haplotypes within a single interval (Figure 4); mixed, with both genotypes present for each polymorphism between the exchange intervals (Figure 5A, 6A); and complex, with two or more haplotype switches, possibly also including both genotypes at some polymorphisms (Figure 5B, 6B).

Simple crossover products were the majority at *C1* in both wild type and *Msh2*$^{-/-}$, but were fewer by ~20% in the mutant (p<0.0001, Fisher's exact test; Figure 3Bi). This reduction primarily reflected an increase in mixed crossovers, which were 23.9% of recombinants in *Msh2*$^{-/-}$. Mixed crossover products would arise from uncorrected heteroduplex DNA in a single crossover product; however, two independent simple crossovers with staggered exchange points in the same well would also appear as a mixed product (Figure S2D). For wild type, the fraction of wells expected to contain two independent recombinants assuming a Poisson distribution (4.1%) is similar to the observed percentage of wells with mixed crossover products (4.5%; p=0.84, Fisher's exact test). For *Msh2*$^{-/-}$, two independent recombinants are expected in a similar percentage of wells (5.0%), but wells with mixed crossover products were observed at a ~5-fold higher frequency (p<0.0001, Fisher's exact test). Thus, most of the mixed crossovers in the absence of MSH2 are expected to be single crossover products with heteroduplex DNA tracts.

Broadly similar results were obtained at *A3*, although simple crossover products, while still predominating, were a smaller fraction of the total in both genotypes. The higher polymorphism density may have led to fewer simple crossover products and/or increased the ability to detect other types. Simple crossover products were again less frequent in *Msh2*$^{-/-}$ ($p<0.0001$, Fisher's exact test; Figure 3Bii). In wild type, mixed crossover products (11%) exceeded the expectation for two independent crossover products in the same well (5.6%; $p=0.0033$, Fisher's exact test), suggesting that some mixed crossover products are single crossover products with uncorrected heteroduplex DNA. In *Msh2*$^{-/-}$, the fraction of mixed crossover products (22.2%) was ~4-fold higher than the Poisson estimate (5.6%; $p<0.0001$, Fisher's exact test), again implying that persistent heteroduplex DNA was more common in the absence of MSH2. For *A3*, the mean minimum mixed tract length from *Msh2*$^{-/-}$ was 252 bp in the D-to-A orientation and 194 bp for A to D (Figure 3C, 6A).

Mixed polymorphisms were observed throughout zones extending ~700 to 800 bp from the hotspot centers, tapering off on both sides (Figure 3B). Limits of these zones may reflect the extent of DMC1 binding (Lange et al., 2016). Mixed polymorphisms were under-represented at the hotspot centers (for example, in *A3* at the four central polymorphisms, which span ~50 bp), and at indels, including the 13 bp indel at *A3* located 250 bp to the left of the hotspot center (Figure 3B).

Tracts with two or more mixed polymorphisms could in principle arise from heteroduplex DNA in which each strand is derived from one parental haplotype, or from heteroduplex DNA in which each strand contains switches between the two haplotypes (Figure S4A) (Hoffmann and Borts, 2005). To distinguish these alternatives, we cloned 29 amplicons containing mixed tracts at *A3* from *Msh2*$^{-/-}$ mice and determined the haplotypes in multiple subclones. Each strand within every mixed tract derived from a single haplotype (Figure S4B). Thus, switches between parental strands in heteroduplex DNA in crossover products are infrequent if they occur at all.

Origin of complex tracts

Complex crossover products were infrequent at *C1*, but were a larger portion of products at *A3* (Figure 3B). As with mixed crossover products, *Msh2*$^{-/-}$ mice had a greater proportion of complex crossover products, e.g., for *A3*, 17.1% in *Msh2*$^{-/-}$ compared with 7.2% in wild type ($p<0.0001$, Fisher's exact test).

Three types of switches between parental haplotypes were observed in the complex crossover products (Figure 3A, types i–iii). For *Msh2*$^{-/-}$ at *A3*, the most common (i) involved just one haplotype switch between the exchange intervals without evidence of heteroduplex retention (43 wells, 54% of complex crossover products) (Figures 3Ai, 6B). These products could not arise from two independent simple crossover products in the same well because none of the polymorphisms were mixed (Figure S3D). Where tested, these complex products yielded identical subclones, confirming the presence of a single complex crossover product (Figure S4B, complex i). Other complex crossover products (ii) had fully converted polymorphisms plus a mixed tract (30 wells, 38% of complex crossover products) (Figure 3Aii). For example in some of these, subcloning showed that one strand had multiple haplotype switches between the exchange intervals, while the other strand had no switches

(Figure S4B, complex ii). The remaining six complex crossover products involved multiple switches of haplotypes without any mixed polymorphisms (8% of complex crossover products; Figure 3Aiii). Although complex crossover products were less frequent in wild type, the observed types were similar.

Complex crossover products could have originated from a continuous heteroduplex tract in which mismatched polymorphisms were corrected in an MSH2-independent manner, for example, by short patch repair (Crown et al., 2014). MSH2-independent correction appeared to be particularly robust at the 13 bp indel in *A3* (Figure 3Bii). Complex tracts were especially frequent to the left of the hotspot center in *A3* where the polymorphism density is high (Figure 6B). We compared the lengths of the mixed and complex tracts at *A3* by focusing on the numerous D-to-A crossover products from *Msh2*$^{-/-}$. Because complex crossover products involve at least two switches between parental haplotypes, we only considered mixed tracts covering at least two polymorphisms. The lengths of these mixed and complex tracts were similar (Figure 3D). Thus, it is conceivable that mixed and complex tracts arise from a common heteroduplex intermediate, but with some products experiencing MSH2-independent correction. Alternatively, complex tracts could arise by other mechanisms, such as template switching, that produces tracts of a similar length.

Crossover patterns provide evidence for biased resolution

To gain insight into mechanisms of recombination, we grouped each type of crossover product according to the position of the exchange relative to the DSB hotspot (shaded in Figures 4–6). At the *C1* hotspot with symmetric DSB formation, a similar number of simple exchanges occurred to the left and to the right of the DSB hotspot for both the A-to-D and D-to-A orientations in wild type and *Msh2*$^{-/-}$ (Figure 4A). Exchanges flanking the mixed tracts in *Msh2*$^{-/-}$ also occurred on either side of the DSB hotspot, although in a few cases the mixed tract spanned the hotspot (Figure 5A). Complex crossover products were too scarce to be informative (Figure 5B).

In contrast, DSBs at *A3* form primarily on the D chromosome, leading to asymmetry in exchange positions. Simple exchanges (Figure 4B) and exchanges flanking the mixed tracts (Figure 6A) occurred primarily to the right of the DSB hotspot in the A-to-D orientation and to the left for the D-to-A orientation. The frequent complex crossover products in the D-to-A orientation showed a similar bias (Figure 6B).

In the simplest version of the canonical model for meiotic recombination, resolution of double Holliday junctions to give rise to crossovers occurs in two configurations, yielding two distinct patterns of heteroduplex DNA (Figure 7A). Considering a DSB on the D chromosome at *A3*, resolution configuration #1 (filled arrowheads) would tend to yield heteroduplex DNA to the left of the DSB hotspot in the D-to-A orientation, while resolution configuration #2 (open arrowheads) would lead to a patch of full conversion to the left of the DSB hotspot and heteroduplex DNA on the right (Figure 7A). Our finding that mixed and complex tracts in the D-to-A orientation were mostly to the left (89 of 110; Figure 6A,B) is therefore consistent with resolution primarily by configuration #1. The fewer mixed and complex tracts on the right side (15 of 110) would also be consistent with resolution configuration #1 when a DSB formed on the A chromosome (Figure S5A). The few

remaining crossover products with mixed and complex tracts that span the DSB hotspot were more ambiguous but constitute only a small fraction of the total (6 of 110). As expected, an opposite bias was obtained in the A-to-D orientation: Mixed and complex tracts were primarily to the right of the DSB hotspot (61 of 72; Figure 6A,B), with few to the left (9 of 72) or spanning the DSB hotspot (2 of 72), again supporting frequent resolution by configuration #1.

In addition to considering the sidedness of the mixed and complex tracts relative to the hotspot center, we also considered the position and length of the mixed tracts within complex crossover products. Resolution configuration #2 without MSH2-independent mismatch repair is predicted to yield a patch of full conversion together with a mixed tract, which is similar in length to mixed tracts generated by resolution configuration #1. Only a few crossover products had this pattern (10 of 182; open arrowheads, Figure 6B), suggesting that this resolution configuration is rare. Moreover, mixed tracts within them typically involved a single polymorphism and thus were much smaller than tracts from mixed crossover products which encompassed multiple polymorphisms (~14-fold smaller, Figure 6C). It is possible that MSH2-independent mismatch correction could operate on many of the products arising from resolution by configuration #2, masking their origin. However, the similar overall mean length of the mixed and complex tracts (Figure 3D) is more consistent with a common intermediate from resolution by configuration #1.

DISCUSSION

Similar meiotic recombination frequencies in wild-type and MSH2-deficient mice

Mammalian meiotic recombination must accommodate sequence differences between alleles without being so permissive as to risk frequent recombination between diverged, yet abundant, non-allelic repeats, which would lead to gross genome instability (Kim et al., 2016). The two hotspots we examined have 0.6% and 1.8% polymorphism density between strains, which apparently is not sufficient to trigger heteroduplex rejection during meiosis, given that both crossover and noncrossover frequencies were largely similar in wild-type and *Msh2*$^{-/-}$ mutant mice. This degree of sequence divergence has been shown to be sufficient to substantially reduce recombination in mouse embryonic stem cells; loss of MSH2 in these cells largely restores recombination levels (de Wind et al., 1995; Elliott and Jasin, 2001; Larocque and Jasin, 2010). Thus, heteroduplex rejection may have a higher threshold for sequence divergence in meiotic cells than in mitotic cells so as not to suppress inter-homolog recombination. A greater tolerance for mismatches may be due the ability of the meiosis-specific recombinase DMC1 to accommodate mismatches within heteroduplex DNA (Lee et al., 2017; Steinfeld et al., 2019).

MSH2 acts to correct heteroduplex DNA in mice

Our data indicate that MSH2 corrects mismatches in meiotic crossover intermediates. Mixed tracts, indicative of heteroduplex DNA retention, were obtained in the absence of MSH2 at a substantial frequency at both hotpots. Complex tracts were similar in length and position to mixed tracts, suggesting that they originated from heteroduplex DNA that was corrected in an MSH2-independent manner. At the less polymorphic *C1* hotspot, mixed and complex

tracts were detected in the absence of MSH2 in 27% of crossover products, while at the highly polymorphic *A3* hotspot, they were detected in nearly 40% of crossover products. The remaining crossover products showed no evidence of a heteroduplex DNA intermediate. The detection of heteroduplex intermediates relies on amplification of both DNA strands; if only one strand were amplified a significant fraction of the time, we would underestimate the frequency of mixed tracts and, hence, heteroduplex DNA. Extrapolation to 100% amplification efficiency, however, still predicts a substantial frequency of simple crossover products (see Methods S1, Supplemental Information).

Another notable finding of our study was the presence of mixed and complex tracts at the *A3* hotspot in wild-type mice, above what would be expected based on Poisson correction for multiple events in a single well. Mixed tracts in wild type differ in that they more often involve only a single polymorphism (42%, 22/53) compared to the mutant (16%, 16/103; p=0.0007, Fisher's exact test). Persistent heteroduplex DNA was also found in meiotic recombination products in wild-type yeast in a genome-wide survey (10% of all events) (Mancera et al., 2011). In normal human sperm, complex patterns have also been detected in crossovers, albeit infrequently (Arbeithuber et al., 2015). All together, this suggests that some mismatches escape detection and repair by MSH2-dependent processes, and this may be more likely at highly polymorphic hotspots like *A3*.

Complex tracts formed in the absence of mismatch repair components have been observed in several organisms (Fleck et al., 1999; Guillon et al., 2005; Martini et al., 2011; Crown et al., 2014). *Mlh1*$^{-/-}$ mice, which unlike *Msh2*$^{-/-}$ mice, are defective in crossover formation as well as canonical mismatch correction, produce a small number of crossovers, and some of these contain both mixed and complex tracts, similar to what we observe in our *Msh2*$^{-/-}$ mice (Guillon et al., 2005; Svetlanov et al., 2008). In fission yeast and *Drosophila* mismatch repair mutants, complex tracts are eliminated when nucleotide excision repair is also disrupted, indicating short patch repair (Fleck et al., 1999; Crown et al., 2014). Short patch repair has also been described in mammalian cell extracts (Krokan et al., 2000; Sugasawa, 2016), which could also be active in meiotic cells in the absence of MSH2. In budding yeast there is no evidence that nucleotide excision repair is linked to the formation of complex tracts in the absence of mismatch repair (Coïc et al., 2000), leading investigators to invoke alternative mechanisms, such as template switching and nick translation, to explain their origin (Marsolier-Kergoat et al., 2018).

Crossover resolution is biased

The crossover patterns we observe suggest that double Holliday junction resolution is biased to favor one of the two hypothetical configurations (filled arrowheads, Figure 7A). In principle, this bias could arise during MLH1-MLH3-dependent resolution of either a fully ligated double Holliday junction or an unligated structure. Resolution in the former case requires four nicks, while resolution in the latter case only requires two nicks. Unlike in mouse, in which ~90% of meiotic crossovers are MLH1-MLH3 dependent (Baker et al., 1996; Woods et al., 1999; Lipkin et al., 2002; Guillon et al., 2005; Svetlanov et al., 2008), a significant fraction of meiotic recombination intermediates in budding yeast are resolved by structure-specific nucleases (Zakharyevich et al., 2012). However, it is notable that the same

resolution bias we observe in mouse has recently been demonstrated for Mlh1-Mlh3-dependent crossovers in yeast (Marsolier-Kergoat et al., 2018).

How crossover resolution bias is achieved is as yet unclear. In principle, nicks or gaps at 3' ends in an unligated double Holliday junction would provide the asymmetry necessary to bias subsequent nicking to favor one crossover configuration (Figure 7A), as has also been proposed for budding yeast and *Drosophila* (Foss et al., 1999; Crown et al., 2014; Marsolier-Kergoat et al., 2018). It is attractive to consider that this same asymmetry could also drive resolution specifically away from generating noncrossovers, given that noncrossovers are known to occur by a distinct pathway from crossovers in mice (Cole et al., 2014). Although less parsimonious, the alternative remains possible that a crossover-to-noncrossover bias is enforced by a different mechanism than a crossover resolution configuration bias (Marsolier-Kergoat et al., 2018).

Alternatively, it has been argued that biased resolution of ligated (or unligated) substrates could be directed by proteins that promote Mlh1-Mlh3-dependent crossing over (Manhart et al., 2017). For example, the first junction formed by strand invasion and repair synthesis could accumulate proteins that stabilize this intermediate, which then direct Mlh1-Mlh3 activity in a preferred configuration, such as PCNA and Msh4-Msh5 (Manhart et al., 2017). Biochemical studies with the yeast complex suggest that it functions in a manner distinct from well-characterized structure-specific nucleases by forming higher order polymer structures (Ranjha et al., 2014; Rogacheva et al., 2014; Claeys Bouuaert and Keeney, 2017; Manhart et al., 2017), which could enforce this bias. Regardless of mechanism, directed resolution of double Holliday junctions appears to restrict the outcome of recombination to one particular crossover configuration, rather than the four possible outcomes (two crossover and two noncrossover) that were originally proposed (Szostak et al., 1983).

Origins of simple crossover products

The original DSB repair model predicts heteroduplex DNA to be present in all intermediates giving rise to crossovers (Szostak et al., 1983) (Figures 7A, S5A). Remarkably, at the highly polymorphic *A3* hotspot, fewer than half of *Msh2*$^{-/-}$ crossover products showed evidence of a heteroduplex intermediate. An MSH2-independent repair process, e.g., short patch repair, could transform a portion of heteroduplex-containing intermediates into both simple and complex crossover products (Figure S6). However, this is unlikely to explain most of the simple crossover products at *A3* since heteroduplex tracts often encompass several polymorphisms, and short patch repair appears to be inefficient as we observe many complex tracts which retain mismatched polymorphisms (Figure 6B).

Instead, our results suggest that heteroduplex DNA is retained on just one chromatid. This could be achieved by D-loop migration, which was initially proposed to explain the absence of some types of aberrant segregation in yeast (Szostak et al., 1983): After strand invasion of one end, DNA repair synthesis moves or extends the D loop past the hotspot center, concomitant with disassembly of heteroduplex DNA arising from strand invasion (Figures 7B, S5B). Alternatively, strand invasion could form only very limited heteroduplex DNA. The heteroduplex DNA that gives rise to mixed tracts when MSH2 is absent would therefore primarily arise from engagement of the second end by the D loop, consistent with findings

from budding yeast in which heteroduplex DNA is physically observed only in later recombination intermediates (Schwacha and Kleckner, 1994; Allers and Lichten, 2001a). Subsequent double Holliday junction resolution results in one simple crossover product and one with heteroduplex DNA. Resolution by configuration #1 is again favored, because it gives rise to heteroduplex DNA with the sidedness that we observe (Figure 7B, S5C).

In this scenario, one or more mechanisms must exist to shift exchange points at the invading end away from the hotspot center without creating heteroduplex DNA, consistent with our observations. For example, gap formation from either 3' to 5' end degradation (Szostak et al., 1983), flap removal after invasion from an interstitial site (Paques and Haber, 1997; Anand et al., 2014) (Figure 7Ci), and/or proofreading by the repair polymerase to degrade the invading strand at mismatches (Anand et al., 2017; Guo et al., 2017) (Figure 7Cii) would all shift the exchange away from the DSB. In these scenarios, the initial invading end and the subsequent "captured" end would undergo distinct processing steps. One prediction is that differential processing could lead to different exchange points for the simple and mixed/complex crossover products. In agreement with this, we observe that exchanges in the simple crossover products are more often outside the hotspot center compared to those from mixed and complex crossover products (Figure S7A, S7B), in that simple crossover products have exchanges which are further from the hotspot center, on average, than mixed or complex crossover products (Figure S7C).

Studies in budding yeast, including recent genome-wide studies in an *msh2Δ* mutant, have also identified crossovers in which heteroduplex DNA was present on one crossover product but not the other, often termed one-sided events (Porter et al., 1993; Gilbertson and Stahl, 1996; Merker et al., 2003; Martini et al., 2011; Marsolier-Kergoat et al., 2018). D-loop migration after strand invasion has also been invoked to explain many of these events. The complexity of meiotic products observed in yeast is enormous, leading to the proposal of a number of other variations to the canonical DSB repair model (Martini et al., 2011; Marsolier-Kergoat et al., 2018). Nonetheless, it is noteworthy that although some aspects of meiotic recombination differ substantially between yeast and mammals, mechanisms of recombination, including biased crossover resolution and D-loop migration leading to one-sided events, appear to be shared.

Concluding remarks

Meiotic recombination has profound effects on genome evolution at many size scales, from cell-wide recombination rates to within-chromosome positioning of crossovers, to fine-scale patterns of mutation and gene conversion near DSB sites. Our results reveal the relative locations of heteroduplex DNA leading to gene conversion and of potentially mutagenic repair DNA synthesis, and the relation of both of these to haplotype exchange points. Further, we show how relative positions of all of these genome-altering events are dictated by crossover resolution bias and D-loop migration. Thus, our findings provide a framework for considering how recombination mechanisms influence genome evolution on a local scale.

STAR METHODS

RESOURCE AVAILABILITY

Lead Contact—Further information and requests for mouse strains and reagents should be directed to the Lead Contact, Maria Jasin (m-jasin@ski.mskcc.org).

Material Availability—*Msh2*$^{tm1Rak/+}$ mice backcrossed to A/J and DBA/2J backrounds are maintained in small numbers; requests for mice will be fulfilled upon request, if possible.

This study did not generate new unique reagents.

Data and Code Availability—Original data including phosphoimager scans of dotblots and all data processing spreadsheets are available from the lead contact upon request.

EXPERIMENTAL MODEL AND SUBJECT DETAILS

Mouse care.—The care and use of mice in this study were performed in accordance with a protocol approved by the Institutional Animal Care and Use Committee (IACUC) at Memorial Sloan Kettering Cancer Center (MSKCC). Mice were housed under Federal regulations and policies governed by the Animal Welfare Act (AWA) and the Health Research Extension Act of 1985 in the Research Animal Resource Center at MSKCC, and was overseen by IACUC.

Mice husbandry, genotyping, and backcrossing.—Wild-type inbred mice were obtained from Jackson Laboratory (A/J stock #000646, DBA/2J stock #000671). *Msh2*$^{tm1Rak/+}$ mice were a gift from W. Edelmann (Smits et al., 2000) and genotyped with a three primer system as described previously (Kovalenko et al., 2012). These mice were originally on a C57BL/6 and 129S mixed background. The *A3* locus was genotyped by restriction digest of two amplicons, Left and Center, which can distinguish the 4 inbred strains:

Left amplicon: Chromosome 1: 160,023,339 –160,025,391

(Relative position to hotspot center: -2394 bp to -342 bp)

A3f3339: 5’ TGTGTCAGGTGAAATAAGGCA 3’

A3r5391: 5’ TCAGTCAGTTGTCAGAGACC 3’

The Left amplicon is digested with StuI and SacI, producing these approximate fragment sizes (bp):129S & A/J: 1000, 650, 400; B6: 1400, 650; DBA/2J: 1650, 400.

Center amplicon: Chromosome 1: 160,025,337–160,026,193

(Relative position to hotspot center: -396 bp to +479 bp)

A3f5337: 5’ TGTTGCCATCCCCAGGGACT 3’

A3r6193: 5’ GATTTGGCCAACATTGTGGG 3’

The Center amplicon is digested with HhaI, producing these approximate fragment sizes (bp): 129S & DBA/2J: 540, 310; A/J & B6: 460, 340, 80.

For *A3* analysis, pair #1 (647 & 648) and pair #2 (651 & 653) were littermates from *Msh2*$^{tm1Rak/+}$ parents, an *A3*$^{A/A}$ dam and *A3*$^{D/D}$ sire. The *A3*$^{A/A}$ dam arose from an *Msh2*$^{tm1Rak/+}$ sire backcrossed with an A/J (*A3*$^{A/A}$) dam for four generations; the *A3*$^{D/D}$ sire arose from a *Msh2*$^{tm1Rak/+}$ dam backcrossed with a DBA/2J (*A3*$^{D/D}$) sire for two generations. The *A3* genotype was verified in the parents by tiled sequencing of a 2.9 kb fragment amplified from tail DNA using universal primers A3f3990 and A3r6911. F1 hybrid littermate pair #3 (1500 & 1501) was obtained from mating an *Msh2*$^{tm1Rak/+}$ *A3*$^{D/D}$ dam derived from a 9-generation DBA/2J backcross and an *Msh2*$^{tm1Rak/+}$ *A3*$^{A/A}$ sire from a 10-generation A/J backcross.

For *C1* analysis, F1 hybrid littermate pair #3 (1500 & 1501) was used, as well as another pair (1674 & 1675) derived from further DBA/2J and A/J backcrosses.

The ages of the experimental male mice at the time of epididymal DNA isolation was:

647(−/−) & 648 (+/+): 17 weeks

651(+/+) & 653 (−/−): 43 weeks

1500(+/+) & 1501 (−/−): 16 weeks

1674(+/+) & 1675 (−/−): 18 weeks

METHOD DETAILS

Isolation of sperm DNA.—Sperm DNA isolation from mice 647, 648, 651 and 653 was performed as described previously (Cole and Jasin, 2011). Sperm DNA isolation from mice 1500, 1501, 1674 & 1675 involved a modified method which led to reduced somatic cell contamination and did not involve enzymatic digestion or differential SDS-lysis of somatic cells. Both caudal and caput epididymides were dissected from >2 month old mice, with all excess fat and tissue trimmed away. A 5 mL tube with cell-strainer cap (BD # 352235) was filled completely with PBS, such that the mesh of the cap was submerged. Epididymides were cut in quarter chunks and placed on top of filter mesh, and submerged in PBS. After 5 minutes, the cap was carefully lifted out of the PBS to break the fluid surface tension, releasing plumes of sperm into the tube. This was repeated every five minutes until sperm were no longer released after lifting out the cap. The cap (and tissue) was removed, and the tube sealed with parafilm. The sperm were pelleted in a swing-bucket rotor for 2 minutes at 4,000 × g. The supernatant was aspirated down to ~1 mL, and then gently resuspended by quick vortex pulses and transferred to a 2 mL screw-cap tube. 5 μL was removed and placed on a slide to access sperm quality and lack of somatic cell contamination. Sperm were then pelleted in a swing-bucket rotor for 5 minutes at 4,000 × g, and the supernatant completely aspirated. Sperm were lysed in 600 μL of lysis buffer (200 mM NaCl, 100 mM Tris-Cl pH 7.5, 5 mM EDTA, 0.5% SDS, 1.5 M 2-mercaptoethanol, 0.5 mg/mL Proteinase K), and resuspended by brief and gentle vortex pulses. Samples were incubated at 55°C for 3–4 hours. DNA was extracted with 600 μL phenol:choloroform, twice. The aqueous phase was

placed in a new tube and DNA was precipitated with 1.2 mL 100% ethanol, and pelleted by centrifuging at 16,000 g for 5 minutes. The pellet was washed with 0.75 mL 70% ethanol, and spun again. The DNA pellet was resuspended in 100 μL 5 mM Tris-Cl, pH 7.5, incubated at 55°C for 1 hour, then overnight at 4°C. DNA was quantified by gel electrophoresis and OD_{260}, and stored in 10 μL aliquots at −20°C.

Crossover and Noncrossover assays.—Experiments were performed as described previously (Cole et al., 2010; Cole and Jasin, 2011). Preliminary experiments were carried out to assess the quality of the template and each allele-specific oligo, by seeding reactions with two copies of each parental haplotype (12 pg hybrid sperm DNA), with an allele-specific oligo and a universal oligo which hybridizes with both haplotypes. For a complete list of all PCR oligonucleotides and Southern probe oligonucleotides used, see Table S3. A Poisson distribution function was applied to determine the number of amplifiable templates seeded in each well, and this adjustment factor was then applied to all subsequent PCRs using the same allele-specific oligo and sperm DNA sample (see Experimental Model and Subject Details, above).

All PCR reactions used 10X “Jeffreys” buffer: 450 mM Tris, pH8.8, 110 mM $(NH_4)_2SO_4$, 45 mM $MgCl_2$, 67 mM 2-mercaptoethanol, 44 μM EDTA, 10 mM each dNTP (Roche, Cat # 3622614001), 1.13 mg/mL ultra-pure (non-acetylated) BSA (Ambion Cat # AM2616), 12.5 mM Tris base (not pH adjusted). Final reaction conditions were as follows: 1X Jeffreys buffer, 0.2 μM each primer, 0.03 U/μL Taq (Thermo Cat # EP0406), 0.006 U/μL Pfu Turbo (Agilent Cat # 600254), in a 10 μL volume. See (Cole and Jasin, 2011) for experimental details, including nested cycling conditions, S1-nuclease digestion, and all other aspects of allele-specific PCR assays and polymorphism genotyping.

To combine data from multiple mice, the Poisson-adjusted crossovers and noncrossovers, and total DNA assayed in each interval from each dataset were summed, with subsequent frequencies and cumulative fractions calculated from these sums after this initial Poisson adjustment.

Tract lengths are always listed as minimum lengths from the first to the last involved polymorphisms.

Clonal analysis of DNA from positive crossover wells.—DNA from crossover PCR reactions containing *Msh2*$^{-/-}$ DNA which were found to contain mixed or complex tracts by Southern dotblotting were TOPO-cloned. Thirty-two individual clones were patch-streaked on agar plates with control clones containing the same amplicon of parental A or D sequence. Patches were replica plated onto several Nylon membranes, cells were lysed by laying the membrane on filter paper soaked in 0.5 M NaCl, 0.5 M NaOH for 2 minutes and neutralized by placing the membrane on filter paper soaked in 1.5 M NaCl, 0.5 M Tris-Cl pH 7.5. The DNA was fixed by drying at room temperature and crosslinking with a Stratalinker. Southern hybridization was performed as described for CO and NCO assays. Note: Some clones were apparently empty vector, while other clones did not transfer, lysed, or became mixed with neighboring patches. Therefore, the total number of clones analyzed was often less than 32 for each well.

Spermatocyte chromosome spreads and Immunofluorescence analysis.— Testes were collected from mice 1500 (WT) & 1501 (*Msh2*$^{-/-}$) and spermatocytes were prepared for surface spreading as previously described (Barchi et al., 2008). SYCP3 (rabbit anti-SYCP3; ab15093; RRID:AB_301639; 1:500) and MLH1 (mouse anti-MLH1; BD Biosciences 554073; RRID:AB_395227; 1:25) were detected by diluting the primary antibodies in dilution buffer (0.2% BSA, 0.2% fish gelatin, 0.05% Triton X-100, 1 × PBS) and incubating overnight at 4 °C. Slides were subsequently washed in dilution buffer three times and incubated with the following secondary antibodies at 1:200 dilution for 1 h at 37 °C: A594 goat anti-rabbit (Thermo A-11012; RRID:AB_2534079) and A488 goat anti-mouse (Thermo A-11001; RRID:AB_2534069). Cover slips were mounted with ProLong Gold antifade reagent with DAPI (Invitrogen P36935).

QUANTIFICATION AND STATISTICAL ANALYSIS

All statistical tests were performed using GraphPad Prism software (https://www.graphpad.com), and the name of the test is indicated in the text or figure legend. For calculating p-values for crossovers and noncrossovers (Table S1 and S2), Fisher's exact test was performed using a 2 × 2 contingency table of the number of Poisson-adjusted crossovers or noncrossovers versus total parental (nonrecombinant) molecules seeded for wild type and *Msh2*$^{-/-}$. For analysis of differences between wild type and *Msh2*$^{-/-}$regarding proportion of mixed or simple wells, the total number of positive wells for each category was used (simple or mixed versus all other positive wells). A post-hoc power analysis was performed using R (version 3.6.3; R Core Team 2020; RRID:SCR_001905) and the pwr.2p.test function from the pwr package (https://CRAN.R-project.org/package=pwr). For the sample sizes in this study (numbers of sperm genomes assayed for each genotype at each hotspot), we estimated 96.2% power to detect an increase in crossover frequency in *Msh2*$^{-/-}$ relative to wild type of 20% or greater (1.2-fold) at the *C1* hotspot, and 99.5% power at *A3*.

Scoring Southern dot blots for crossover and noncrossover genotyping.— Each dot blot included a control dilution series of the haplotype being probed: 100%, 1:10, 1:30, 1:100, 1:300, and 1:1000 of the control haplotype DNA was diluted into DNA of the opposite haplotype. Blots were imaged with a phosphoimager (GE Typhoon 7000), and the intensity of each dot was quantified in Image J (https://imagej.nih.gov/ij/). A standard curve was created, and the intensity of each experimental dot was compared to this curve, with only signals surpassing the 1:30 dilution being considered positive.

Supplementary Material

Refer to Web version on PubMed Central for supplementary material.

ACKNOWLEDGEMENTS

The authors would like to thank Shintaro Yamada, Francesca Cole, Julian Lange, and members of the Jasin and Keeney labs for assistance and discussions. This work was supported by MSK Cancer Center Support Grant/Core Grant (NIH P30CA008748), a Tri-I Starr Stem Cell fellowship (SEP), R35 GM118092 (SK), and R35 GM118175 (MJ).

REFERENCES

Allers T, and Lichten M (2001a). Differential timing and control of noncrossover and crossover recombination during meiosis. Cell 106, 47–57. [PubMed: 11461701]

Allers T, and Lichten M (2001b). Intermediates of yeast meiotic recombination contain heteroduplex DNA. Mol. Cell 8, 225–231. [PubMed: 11511375]

Anand R, Beach A, Li K, and Haber J (2017). Rad51-mediated double-strand break repair and mismatch correction of divergent substrates. Nature 544, 377–380. [PubMed: 28405019]

Anand RP, Tsaponina O, Greenwell PW, Lee C-S, Du W, Petes TD, and Haber JE (2014). Chromosome rearrangements via template switching between diverged repeated sequences. Genes Dev. 28, 2394–2406. [PubMed: 25367035]

Anderson CM, Oke A, Yam P, Zhuge T, and Fung JC (2015). Reduced Crossover Interference and Increased ZMM-Independent Recombination in the Absence of Tel1/ATM. PLoS Genet 11, e1005478. [PubMed: 26305689]

Arbeithuber B, Betancourt AJ, Ebner T, and Tiemann-Boege I (2015). Crossovers are associated with mutation and biased gene conversion at recombination hotspots. Proc. Natl. Acad. Sci. U. S. A 112, 2109–2114. [PubMed: 25646453]

Baker SM, Plug AW, Prolla TA, Bronner CE, Harris AC, Yao X, Christie DM, Monell C, Arnheim N, Bradley A, et al. (1996). Involvement of mouse Mlh1 in DNA mismatch repair and meiotic crossing over. Nat. Genet 13, 336–342. [PubMed: 8673133]

Barchi M, Roig I, Di Giacomo M, de Rooij DG, Keeney S, and Jasin M (2008). ATM promotes the obligate XY crossover and both crossover control and chromosome axis integrity on autosomes. PLoS Genet. 4, e1000076. [PubMed: 18497861]

Borts RH, Chambers SR, and Abdullah MF (2000). The many faces of mismatch repair in meiosis. Mutat. Res 451, 129–150. [PubMed: 10915869]

Chakraborty U, and Alani E (2016). Understanding how mismatch repair proteins participate in the repair/anti-recombination decision. FEMS Yeast Res 16, fow071. [PubMed: 27573382]

Chen SY, Tsubouchi T, Rockmill B, Sandler JS, Richards DR, Vader G, Hochwagen A, Roeder GS, and Fung JC (2008). Global analysis of the meiotic crossover landscape. Dev. Cell 15, 401–415. [PubMed: 18691940]

Chen W, and Jinks-Robertson S (1999). The role of the mismatch repair machinery in regulating mitotic and meiotic recombination between diverged sequences in yeast. Genetics 151, 1299–1313. [PubMed: 10101158]

Claeys Bouuaert C, and Keeney S (2017). Distinct DNA-binding surfaces in the ATPase and linker domains of MutLγ determine its substrate specificities and exert separable functions in meiotic recombination and mismatch repair. PLoS Genet. 13, e1006722. [PubMed: 28505149]

Coïc E, Gluck L, and Fabre F (2000). Evidence for short-patch mismatch repair in Saccharomyces cerevisiae. EMBO J. 19, 3408–3417. [PubMed: 10880453]

Cole F, Baudat F, Grey C, Keeney S, de Massy B, and Jasin M (2014). Mouse tetrad analysis provides insights into recombination mechanisms and hotspot evolutionary dynamics. Nat Genet 46, 1072–1080. [PubMed: 25151354]

Cole F, and Jasin M (2011). Isolation of meiotic recombinants from mouse sperm. Methods Mol. Biol 745, 251–282. [PubMed: 21660699]

Cole F, Keeney S, and Jasin M (2010). Comprehensive, fine-scale dissection of homologous recombination outcomes at a hot spot in mouse meiosis. Mol. Cell 39, 700–710. [PubMed: 20832722]

Collins I, and Newlon CS (1994). Meiosis-specific formation of joint DNA molecules containing sequences from homologous chromosomes. Cell 76, 65–75. [PubMed: 8287480]

Crown KN, McMahan S, and Sekelsky J (2014). Eliminating both canonical and short-patch mismatch repair in Drosophila melanogaster suggests a new meiotic recombination model. PLoS Genet. 10, e1004583. [PubMed: 25188408]

Dapper AL, and Payseur BA (2017). Connecting theory and data to understand recombination rate evolution. Philos Trans R Soc Lond B Biol Sci 372.

Datta A, Adjiri A, New L, Crouse GF, and Jinks Robertson S (1996). Mitotic crossovers between diverged sequences are regulated by mismatch repair proteins in Saccaromyces cerevisiae. Mol Cell Biol 16, 1085–1093. [PubMed: 8622653]

de Boer E, Jasin M, and Keeney S (2015). Local and sex-specific biases in crossover vs. noncrossover outcomes at meiotic recombination hot spots in mice. Genes Dev. 29, 1721–1733. [PubMed: 26251527]

de Wind N, Dekker M, Berns A, Radman M, and te Riele H (1995). Inactivation of the mouse Msh2 gene results in mismatch repair deficiency, methylation tolerance, hyperrecombination, and predisposition to cancer. Cell 82, 321–330. [PubMed: 7628020]

Elliott B, and Jasin M (2001). Repair of double-strand breaks by homologous recombination in mismatch repair-defective mammalian cells. Mol. Cell. Biol 21, 2671–2682. [PubMed: 11283247]

Fleck O, Lehmann E, Schär P, and Kohli J (1999). Involvement of nucleotide-excision repair in msh2 pms1-independent mismatch repair. Nat. Genet 21, 314–317. [PubMed: 10080187]

Foss HM, Hillers KJ, and Stahl FW (1999). The conversion gradient at HIS4 of Saccharomyces cerevisiae. II. A role for mismatch repair directed by biased resolution of the recombinational intermediate. Genetics 153, 573–583. [PubMed: 10511540]

Gilbertson LA, and Stahl FW (1996). A test of the double-strand break repair model for meiotic recombination in Saccharomyces cerevisiae. Genetics 144, 27–41. [PubMed: 8878671]

Gray S, and Cohen PE (2016). Control of Meiotic Crossovers: From Double-Strand Break Formation to Designation. Annu. Rev. Genet 50, 175–210. [PubMed: 27648641]

Guillon H, Baudat F, Grey C, Liskay RM, and de Massy B (2005). Crossover and noncrossover pathways in mouse meiosis. Mol. Cell 20, 563–573. [PubMed: 16307920]

Guo X, Hum YF, Lehner K, and Jinks-Robertson S (2017). Regulation of hetDNA Length during Mitotic Double-Strand Break Repair in Yeast. Mol. Cell 67, 539–549 e534. [PubMed: 28781235]

Hoffmann ER, and Borts RH (2005). Trans events associated with crossovers are revealed in the absence of mismatch repair genes in Saccharomyces cerevisiae. Genetics 169, 1305–1310. [PubMed: 15654113]

Hunter N (2015). Meiotic Recombination: The Essence of Heredity. Cold Spring Harb. Perspect. Biol 7.

Kim S, Peterson SE, Jasin M, and Keeney S (2016). Mechanisms of germ line genome instability. Semin. Cell Dev. Biol 54, 177–187. [PubMed: 26880205]

Kovalenko M, Dragileva E, St Claire J, Gillis T, Guide JR, New J, Dong H, Kucherlapati R, Kucherlapati MH, Ehrlich ME, et al. (2012). Msh2 acts in medium-spiny striatal neurons as an enhancer of CAG instability and mutant huntingtin phenotypes in Huntington's disease knock-in mice. PLoS One 7, e44273. [PubMed: 22970194]

Krokan HE, Nilsen H, Skorpen F, Otterlei M, and Slupphaug G (2000). Base excision repair of DNA in mammalian cells. FEBS Lett 476, 73–77. [PubMed: 10878254]

Lam I, and Keeney S (2015). Mechanism and regulation of meiotic recombination initiation. Cold Spring Harb. Perspect. Biol 7, a016634.

Lange J, Yamada S, Tischfield SE, Pan J, Kim S, Zhu X, Socci ND, Jasin M, and Keeney S (2016). The Landscape of Mouse Meiotic Double-Strand Break Formation, Processing, and Repair. Cell 167, 695–708.e616. [PubMed: 27745971]

Larocque JR, and Jasin M (2010). Mechanisms of recombination between diverged sequences in wild-type and BLM-deficient mouse and human cells. Mol. Cell. Biol 30, 1887–1897. [PubMed: 20154148]

Lee JY, Steinfeld JB, Qi Z, Kwon Y, Sung P, and Greene EC (2017). Sequence imperfections and base triplet recognition by the Rad51/RecA family of recombinases. J. Biol. Chem 292, 11125–11135. [PubMed: 28476890]

Lipkin SM, Moens PB, Wang V, Lenzi M, Shanmugarajah D, Gilgeous A, Thomas J, Cheng J, Touchman JW, Green ED, et al. (2002). Meiotic arrest and aneuploidy in MLH3-deficient mice. Nat. Genet 31, 385–390. [PubMed: 12091911]

Mancera E, Bourgon R, Brozzi A, Huber W, and Steinmetz LM (2008). High-resolution mapping of meiotic crossovers and non-crossovers in yeast. Nature 454, 479–485. [PubMed: 18615017]

Mancera E, Bourgon R, Huber W, and Steinmetz LM (2011). Genome-wide survey of post-meiotic segregation during yeast recombination. Genome Biol 12, R36. [PubMed: 21481229]

Manhart CM, Ni X, White MA, Ortega J, Surtees JA, and Alani E (2017). The mismatch repair and meiotic recombination endonuclease Mlh1-Mlh3 is activated by polymer formation and can cleave DNA substrates in trans. PLoS Biol. 15, e2001164. [PubMed: 28453523]

Marsolier-Kergoat MC, Khan MM, Schott J, Zhu X, and Llorente B (2018). Mechanistic View and Genetic Control of DNA Recombination during Meiosis. Mol Cell 70, 9–20. [PubMed: 29625041]

Martini E, Borde V, Legendre M, Audic S, Regnault B, Soubigou G, Dujon B, and Llorente B (2011). Genome-wide analysis of heteroduplex DNA in mismatch repair-deficient yeast cells reveals novel properties of meiotic recombination pathways. PLoS Genet. 7, e1002305. [PubMed: 21980306]

McMahill MS, Sham CW, and Bishop DK (2007). Synthesis-dependent strand annealing in meiosis. PLoS Biol 5, e299. [PubMed: 17988174]

Merker JD, Dominska M, and Petes TD (2003). Patterns of heteroduplex formation associated with the initiation of meiotic recombination in the yeast Saccharomyces cerevisiae. Genetics 165, 47–63. [PubMed: 14504217]

Paques F, and Haber JE (1997). Two pathways for removal of nonhomologous DNA ends during double-strand break repair in Saccharomyces cerevisiae. Mol Cell Biol 17, 6765–6771. [PubMed: 9343441]

Porter SE, White MA, and Petes TD (1993). Genetic evidence that the meiotic recombination hotspot at the HIS4 locus of Saccharomyces cerevisiae does not represent a site for a symmetrically processed double-strand break. Genetics 134, 5–19. [PubMed: 8514148]

Pratto F, Brick K, Khil P, Smagulova F, Petukhova GV, and Camerini-Otero RD (2014). DNA recombination. Recombination initiation maps of individual human genomes. Science 346, 1256442. [PubMed: 25395542]

Ranjha L, Anand R, and Cejka P (2014). The Saccharomyces cerevisiae Mlh1-Mlh3 heterodimer is an endonuclease that preferentially binds to Holliday junctions. J. Biol. Chem 289, 5674–5686. [PubMed: 24443562]

Rogacheva MV, Manhart CM, Chen C, Guarne A, Surtees J, and Alani E (2014). Mlh1-Mlh3, a meiotic crossover and DNA mismatch repair factor, is a Msh2-Msh3-stimulated endonuclease. J. Biol. Chem 289, 5664–5673. [PubMed: 24403070]

Schwacha A, and Kleckner N (1994). Identification of joint molecules that form frequently between homologs but rarely between sister chromatids during yeast meiosis. Cell 76, 51–63. [PubMed: 8287479]

Schwacha A, and Kleckner N (1995). Identification of double Holliday junctions as intermediates in meiotic recombination. Cell 83, 783–791. [PubMed: 8521495]

Smits R, Hofland N, Edelmann W, Geugien M, Jagmohan-Changur S, Albuquerque C, Breukel C, Kucherlapati R, Kielman MF, and Fodde R (2000). Somatic Apc mutations are selected upon their capacity to inactivate the beta-catenin downregulating activity. Genes Chromosomes Cancer 29, 229–239. [PubMed: 10992298]

Spencer CC, Deloukas P, Hunt S, Mullikin J, Myers S, Silverman B, Donnelly P, Bentley D, and McVean G (2006). The influence of recombination on human genetic diversity. PLoS Genet 2, e148. [PubMed: 17044736]

Spies M, and Fishel R (2015). Mismatch repair during homologous and homeologous recombination. Cold Spring Harb. Perspect. Biol 7, a022657. [PubMed: 25731766]

Steinfeld JB, Belan O, Kwon Y, Terakawa T, Al-Zain A, Smith MJ, Crickard JB, Qi Z, Zhao W, Rothstein R, et al. (2019). Defining the influence of Rad51 and Dmc1 lineage-specific amino acids on genetic recombination. Genes Dev 33, 1191–1207. [PubMed: 31371435]

Sugasawa K (2016). Molecular mechanisms of DNA damage recognition for mammalian nucleotide excision repair. DNA Repair (Amst) 44, 110–117. [PubMed: 27264556]

Svetlanov A, Baudat F, Cohen PE, and de Massy B (2008). Distinct functions of MLH3 at recombination hot spots in the mouse. Genetics 178, 1937–1945. [PubMed: 18430927]

Szostak JW, Orr-Weaver TL, Rothstein RJ, and Stahl FW (1983). The double-strand-break repair model for recombination. Cell 33, 25–35. [PubMed: 6380756]

Tham K-C, Kanaar R, and Lebbink JHG (2016). Mismatch repair and homeologous recombination. DNA Repair 38, 75–83. [PubMed: 26739221]

Veller C, Kleckner N, and Nowak MA (2019). A rigorous measure of genome-wide genetic shuffling that takes into account crossover positions and Mendel's second law. Proc. Natl. Acad. Sci. U. S. A 116, 1659–1668. [PubMed: 30635424]

Woods LM, Hodges CA, Baart E, Baker SM, Liskay M, and Hunt PA (1999). Chromosomal influence on meiotic spindle assembly: abnormal meiosis I in female Mlh1 mutant mice. J. Cell Biol 145, 1395–1406. [PubMed: 10385520]

Wu L, and Hickson ID (2003). The Bloom's syndrome helicase suppresses crossing over during homologous recombination. Nature 426, 870–874. [PubMed: 14685245]

Zakharyevich K, Tang S, Ma Y, and Hunter N (2012). Delineation of joint molecule resolution pathways in meiosis identifies a crossover-specific resolvase. Cell 149, 334–347. [PubMed: 22500800]

Highlights

Highlights are 3–4 bullet points of no more than 85 characters in length, including spaces, and they summarize the core results of the paper in order to allow readers to quickly gain an understanding of the main take-home messages.

- Fine-scale mapping of heteroduplex DNA in mismatch repair-defective mice.
- Mismatch repair-mediated heteroduplex rejection is not evident during meiosis.
- Heteroduplex DNA patterns revise the canonical meiotic recombination model in mice.
- D-loop migration & asymmetric Holliday junction cleavage are intrinsic features.

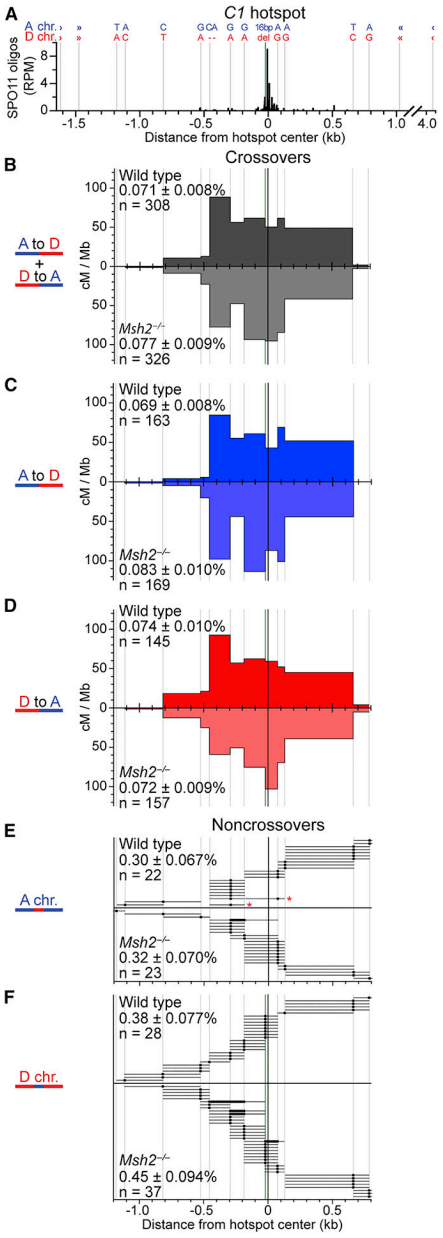

Figure 1. Meiotic recombination frequency and distribution are unaffected by MSH2 at *C1*—a symmetric hotspot with low polymorphism density.

(A) The hotspot center is defined by SPO11 oligos obtained from B6 mice. Polymorphisms are indicated by vertical lines (green for the indel), with genotypes indicated above. Nested allele-specific forward and reverse primers are indicated by angle brackets. (**B–D**) Exchange interval maps for total (panel B), A-to-D (panel C), and D-to-A (panel D) crossovers. (**E and F**) Individual noncrossover gene conversion tracts, plotted on a per-well basis, for conversions on the A chromosome to D sequence **(E)**, or vice versa **(F)**. Thick dots and bars are converted polymorphisms, thin lines are the maximum possible tract lengths to the next unconverted polymorphism. Colored asterisks indicate wells showing conversion of non-contiguous polymorphisms. In B–F, Poisson-corrected frequencies are indicated ± SD; n = number of positive wells.

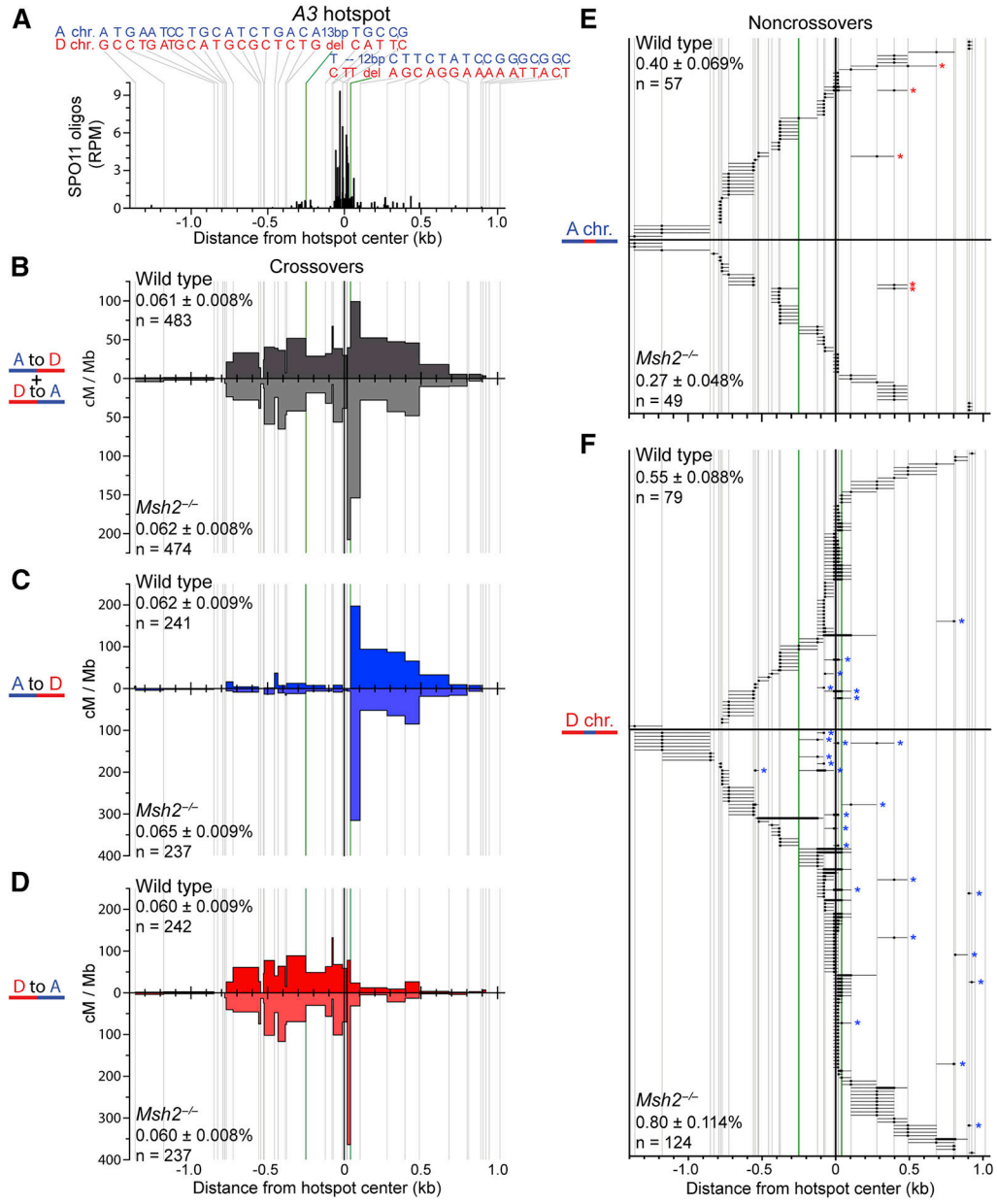

Figure 2. Meiotic Recombination Frequency and Distribution Are Unaffected by MSH2 at A3–An Asymmetric Hotspot with High Polymorphism Density

(A) Hotspot schematic, as in Figure 1A. For genotypes shown at top, commas separate closely spaced SNPs detected in the same allele-specific oligonucleotide. (B–F) Exchange point maps (B–D) and noncrossover gene conversions (E and F) are shown as described in the legend to Figure 1.

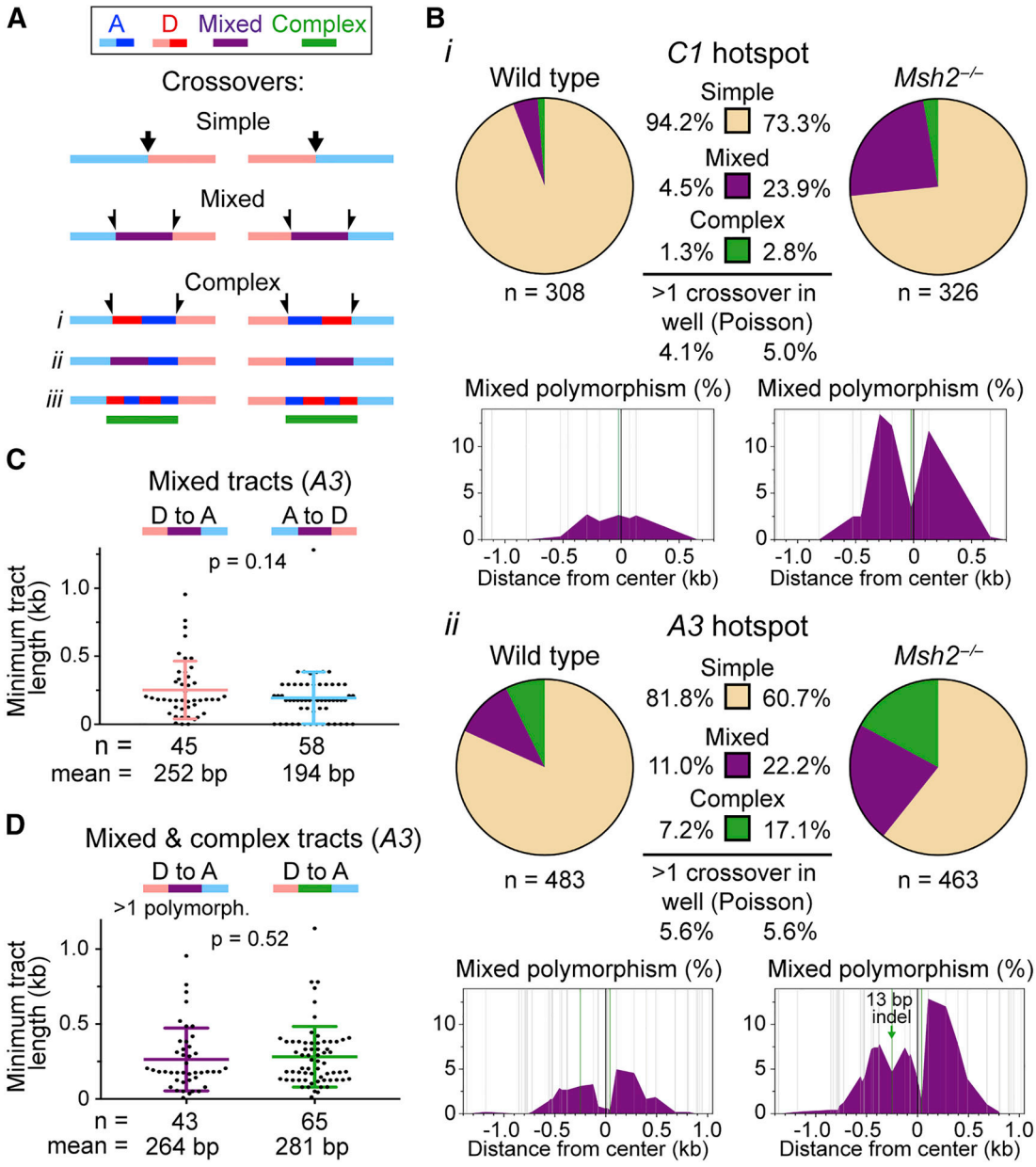

Figure 3. Mixed and Complex Crossover Products Are More Frequent in the Absence of MSH2 and Likely Arise from the Same Heteroduplex Intermediate

(A) Crossover products were grouped into three classes: simple, mixed, and complex, with representative depictions in both A-to-D and D-to-A orientations. Exchange points, indicated by arrows, were used to calculate interval-specific recombination rates and the maps of Figures 1 and 2. Simple crossover products have a single exchange interval. For the mixed and complex crossover products, we assigned half an exchange to each interval flanking the mixed or complex tract. For complex crossover products, three sub-types were identified: (i) those containing a haplotype switch between the exchange intervals, without any mixed polymorphisms; (ii) those containing at least one mixed polymorphism; and (iii) those containing more than two haplotype switches, without any mixed polymorphisms. In this and subsequent figures, a horizontal purple bar represents a mixed tract and a horizontal

green bar represents a complex tract, flanked by parental sequence (represented as light blue and pink). (B) The proportions of simple, mixed, or complex crossover products at C1 (i) and A3 (ii) in wild-type and Msh2$^{-/-}$ mice (two mice of each genotype for C1 and three for A3). n = total crossover products. The Poisson-predicted percentages of positive wells expected to contain more than one crossover product are indicated below. Maps showing the fraction of mixed polymorphisms within the entire population of crossover products across the hotspot for each genotype are shown below each pie chart. (C) The minimum length of mixed tracts at the A3 hotspot from Msh2$^{-/-}$ mice was plotted separately for the D-to-A and A-to-D orientations. Means are shown ± SD. The lengths are not significantly different. (D) The minimum lengths of D-to-A mixed tracts consisting of more than 1 polymorphism were similar to the minimum lengths of all D-to-A complex tracts at A3 from Msh2$^{-/-}$ mice. Means are shown ± SD. p values in (C) and (D) from Mann-Whitney tests.

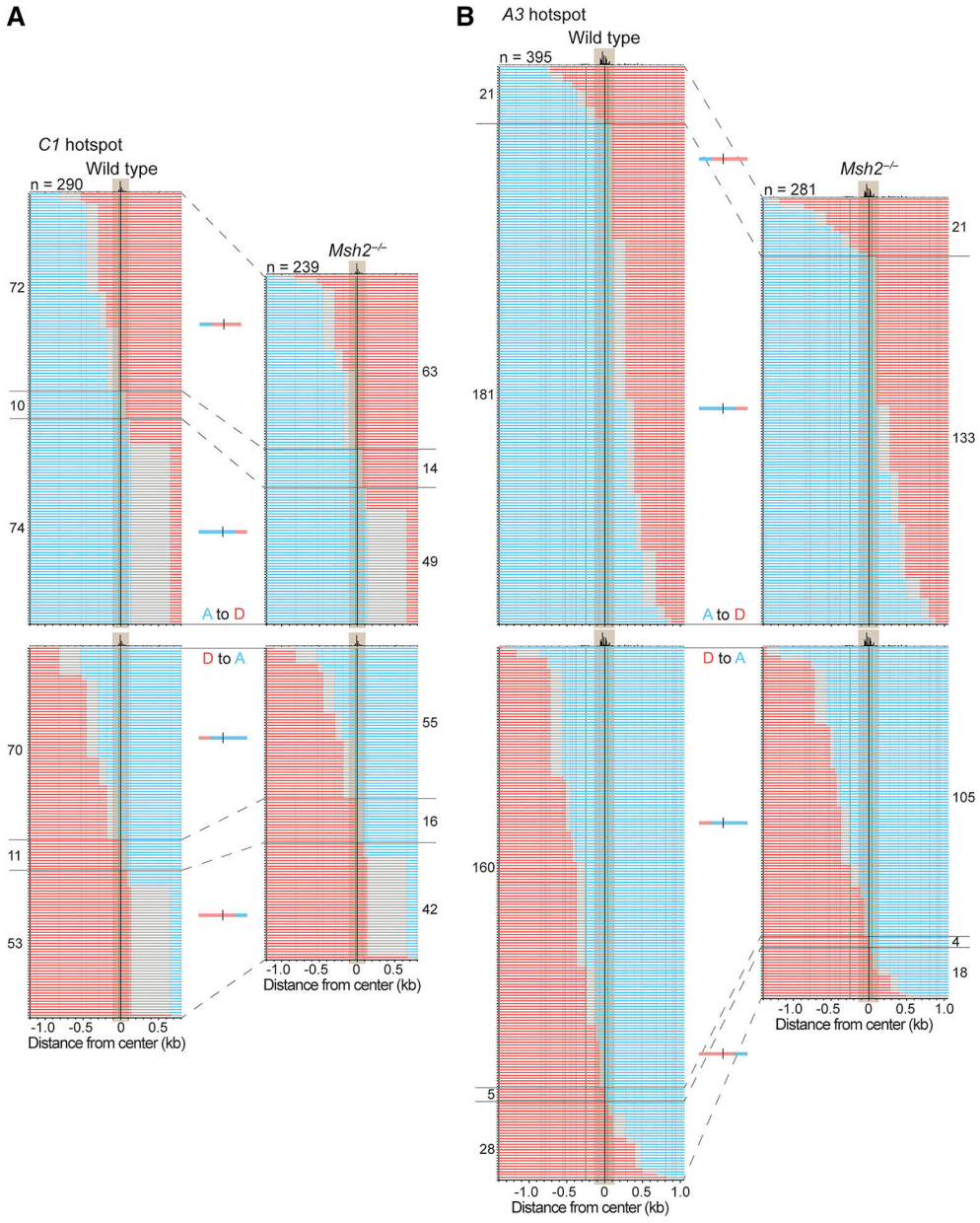

Figure 4. Simple crossover products.

The haplotype of each crossover product at *C1* **(A)** and *A3* **(B)** is plotted horizontally, ordered by the position of exchange, with A-to-D crossovers on the top. Exchange intervals are in gray. Schematics depict four types of simple crossover products (from top to bottom): A to D with an exchange to the left of the hotspot center, A to D with an exchange to the right of the hotspot center, D to A with an exchange to the left of the hotspot center, and D to A with an exchange to the right of the hotspot center. Total numbers of simple crossovers are indicated (n). The number of crossover products in each group is indicated to the left (wild type) or right (*Msh2*$^{-/-}$) of the plots. A map of SPO11 oligos (DSBs) is at the top of each stack, with the DSB hotspot shaded throughout the crossover stack (200 bp wide at *C1*, 250 bp wide at *A3*).

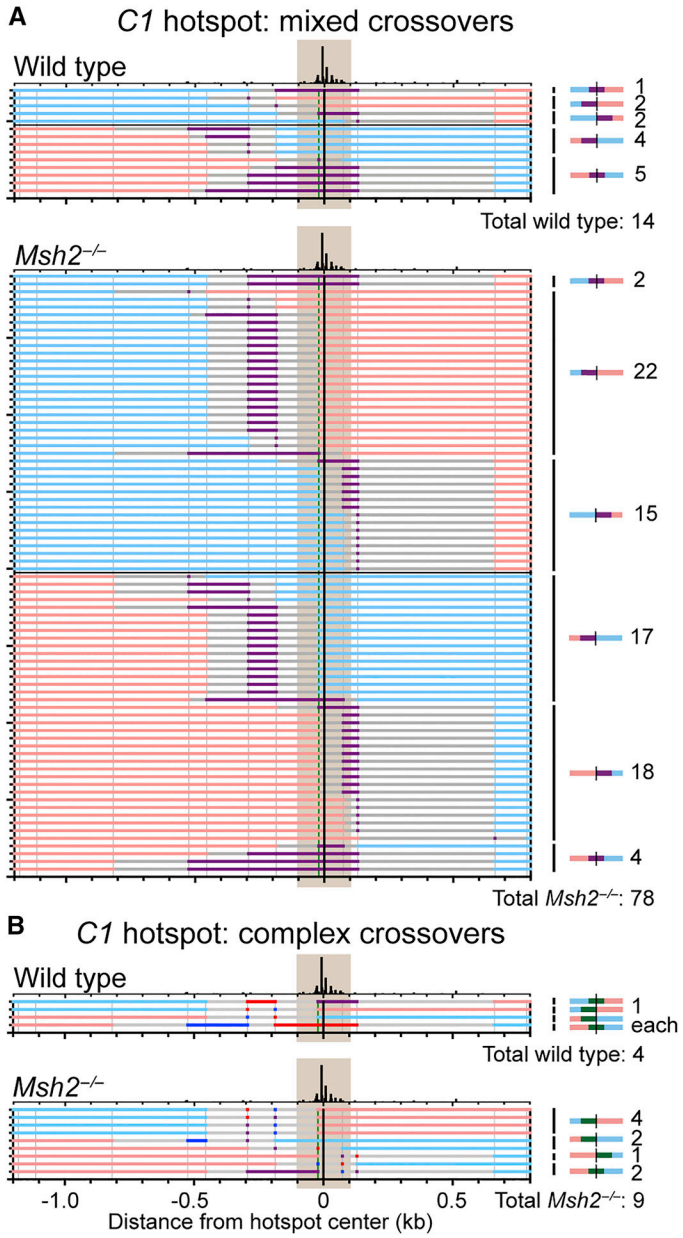

Figure 5. Mixed and complex crossover products from the *C1* hotspot.

Wild-type and *Msh2*$^{-/-}$ mixed **(A)** and complex **(B)** crossover products from *C1* are plotted as in Figure 4, with A-to-D crossover products on top. Mixed polymorphisms/tracts are indicated in purple. Schematics on the right depict the position of the mixed (purple) or complex tracts (green) within the A-to-D or D-to-A crossover products: to the left, right, or spanning the DSB hotspot, with the number of crossover products of each type indicated next to the schematic. Total numbers of mixed/complex crossover products are indicated under each panel.

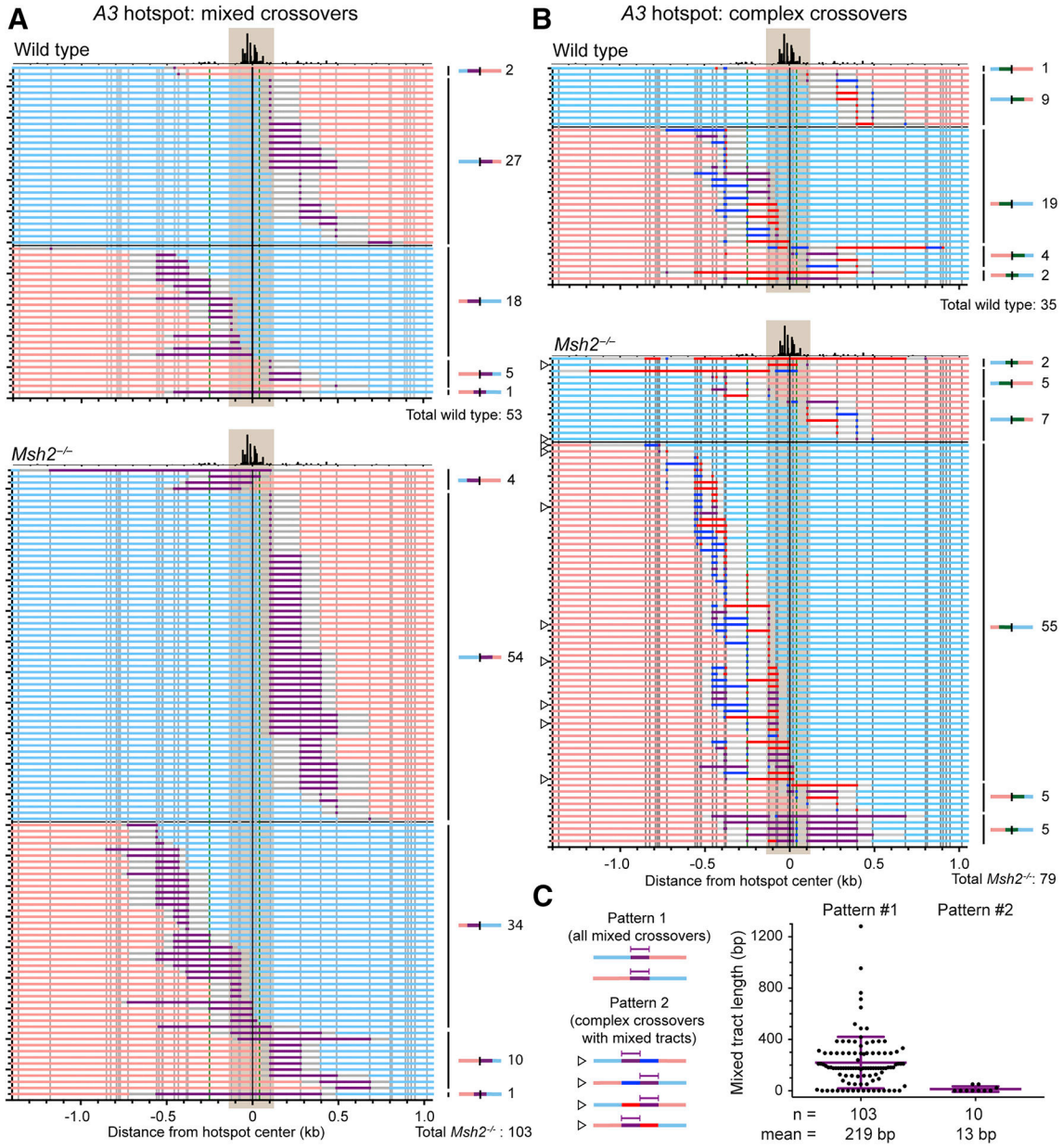

Figure 6. Mixed and complex crossover products from the *A3* hotspot.

Wild-type and *Msh2*$^{-/-}$ mixed **(A)** and complex **(B)** crossover products from *A3* are plotted as in Figure 5. Open arrowheads indicate the complex crossovers in *Msh2*$^{-/-}$ that potentially conform to pattern 2 in Figure 7A. **(C)** The minimum mixed tract lengths at *A3* in *Msh2*$^{-/-}$ mice are plotted for mixed crossover products which conform to pattern 1 and for complex crossover products which could potentially conform to pattern 2 (indicated by open arrowheads in B). Most mixed tracts from pattern 2 encompassed just a single polymorphism, and were on average 14.5-fold shorter than the mixed tracts from pattern 1 ($p \leq 0.0001$, Mann-Whitney test).

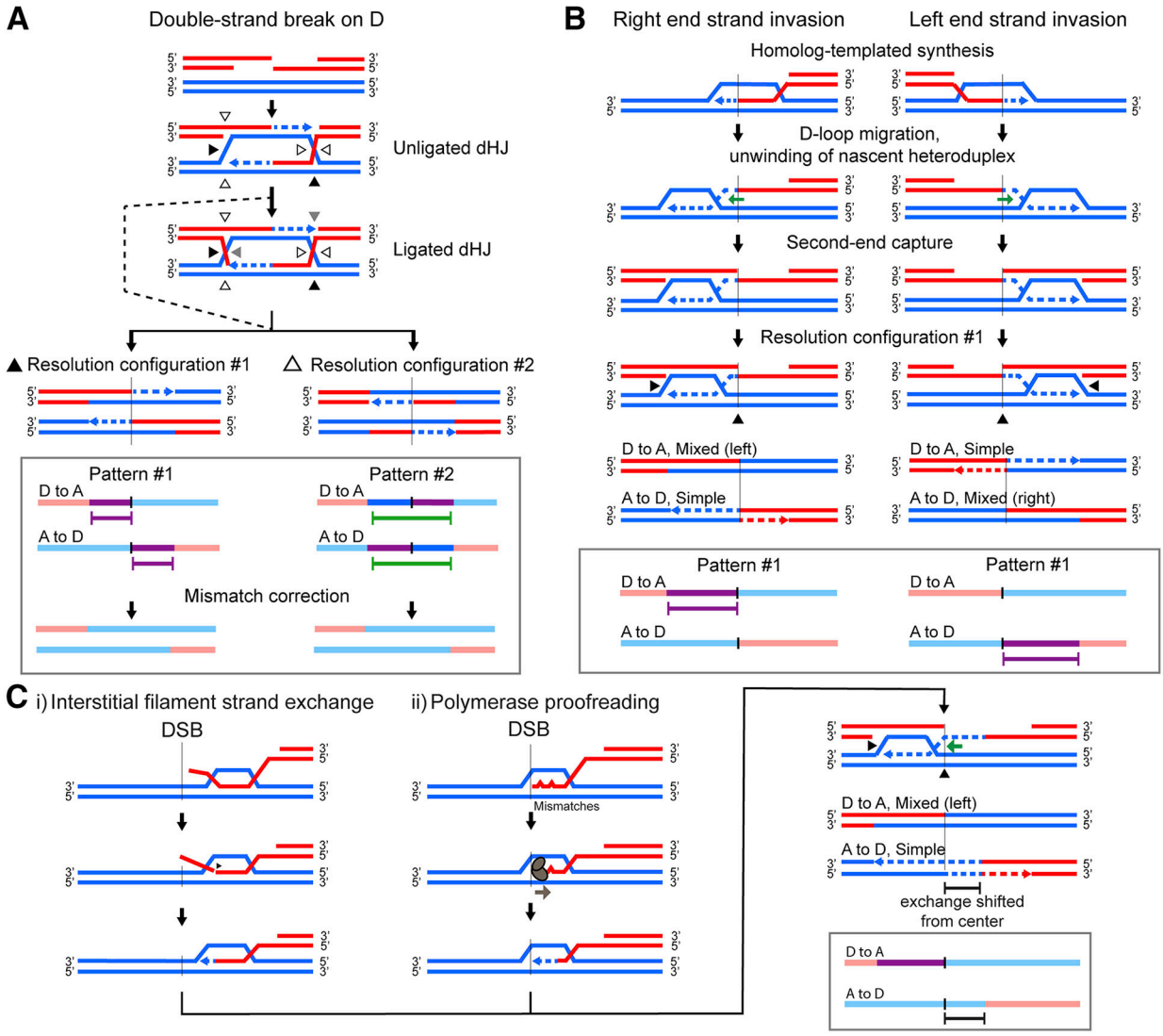

Figure 7. Canonical and modified models for meiotic crossover formation.

(A) The canonical DSB repair model. A break on the D chromosome or the A chromosome (Figure S5A) leads to resection, strand invasion, and second end capture. This intermediate may mature into a fully ligated double Holliday junction (dHJ), or may be acted on by resolvases with nicks still present (dashed pathway). Single-strand cleavage at the four (ligated dHJ) or two (unligated dHJ) filled arrowheads will yield crossover pattern #1, while cleavage at the four open arrowheads will yield crossover pattern #2. The downward arrows and vertical black lines indicate the DSB position. Below these products are schematic representations of crossovers with mixed tracts indicated by purple brackets and complex tracts indicated by green brackets. Below this is the pattern that would be expected in wild type after mismatch correction. **(B)** D-loop migration model to account for abundance of simple crossovers. Initial strand invasion from each end is shown separately, yielding different crossover products. After strand exchange, repair synthesis and strand unwinding causes co-directional D-loop migration, so that the D-loop ends up on one side of the break. Subsequent second-end capture by the D-loop creates a new heteroduplex tract, and

resolution of the double-Holliday junction by configuration #1 will produce one simple crossover product and one with a heteroduplex DNA tract. With frequent breaks on the D chromosome at the *A3* hotspot, this simple model can produce crossovers with the patterns we observe, namely, many simple crossovers, D-to-A crossovers with a mixed tract to the left of the hotspot, and A-to-D crossovers with a mixed tract to the right. **(C)** Alterations to the model presented in (B) that shift the simple crossover exchanges away from the hotspot center. (*i*) Strand exchange at an interstitial position of the DMC1/RAD51 nucleoprotein filament, followed by cleavage of the distal 3' ssDNA end. Repair synthesis proceeds from the clipped end, causing the exchange in the simple crossover product to be shifted away from the hotspot center. *(ii)* The repair DNA polymerase can detect mismatches at the 3' end of the invaded strand, which will ultimately cause the exchange to be modestly shifted away from the center in the resulting simple crossover. The crossover with heteroduplex DNA has an exchange point defined by the 3' end of the non-invading broken strand, or, by the position/length of the D-loop prior to resolution.

KEY RESOURCES TABLE

REAGENT or RESOURCE	SOURCE	IDENTIFIER
Antibodies		
mouse anti-MLH1	BD Biosciences	554073; RRID:AB_395227
rabbit anti-SYCP3	Abcam	ab15093; RRID:AB_301639
goat anti-mouse A488	Thermo	A-11001; RRID:AB_2534069
goat anti-rabbit A594	Thermo	A-11012; RRID:AB_2534079
Chemicals, Peptides, and Recombinant Proteins		
Taq DNA polymerase	Thermo	Cat # EP0406
Pfu Turbo DNA polymerase	Agilent	Cat # 600254
Non-acetylated ultra-pure bovine serum albumin (BSA)	Ambion	Cat # AM2616
dNTPs, PCR-grade	Roche	Cat # 3622614001
Experimental Models: Organisms/Strains		
Msh2$^{tm1Rak/+}$ heterozygous mice (referred to as Msh2$^{+/-}$)	Smits, et. al., 2000.	RRID:MGI:4355514
Inbred A/J mice for backcrossing *Msh2*$^{+/-}$ mice	The Jackson Laboratory	Strain # 000646; RRID:IMSR_JAX:000646
Inbred DBA/2J mice for backcrossing *Msh2*$^{+/-}$ mice	The Jackson Laboratory	Strain # 000671; RRID:IMSR_JAX:000671
Oligonucleotides		
All oligos used for PCR assays and Southern dot blotting, See Supplemental Information, Table S3.	Integrated DNA Technologies (IDT), Eton Biosciences	
Software and Algorithms		
Data analysis and graphical presentation	GraphPad Prism 7	RRID:SCR_002798
Quantification of dot blots	Image J	RRID:SCR_003070
Calculation of recombination frequencies and other data	Microsoft Excel	RRID:SCR_016137
R project for statistical computing	http://www.r-project.org	RRID:SCR_001905
Pwr (R package): Basic functions for Power Analysis	Htpps://CRAN.R-project.org/package=pwr	n/a